Colloid phase separation dynamics driven by chiral turbulent flows

Jiaxing Yuan [1] and Hajime Tanaka [1,2,*]

[1]*Research Center for Advanced Science and Technology, University of Tokyo, 4-6-1 Komaba, Meguro-ku, Tokyo 153-8904, Japan*

[2]*Department of Fundamental Engineering, Institute of Industrial Science, University of Tokyo, 4-6-1 Komaba, Meguro-ku, Tokyo 153-8505, Japan*

(Received 8 November 2023; revised 9 February 2024; accepted 25 April 2024; published 20 May 2024)

Hydrodynamic interactions significantly influence phase-ordering kinetics in complex fluids. While passive fluid phase separation is well studied, the impact of active components remains relatively unexplored. We examine pure- and quasi-two-dimensional mixtures of attractive colloids and self-rotating particles in a solvent. Varying rotor rotational speed and area fraction yield diverse dynamic patterns such as percolated networks and round droplets composed of passive colloids alone. At intermediate rotation speeds, inertial chiral flows, accompanied by the inverse energy cascade, lead to self-similar power-law coarsening with a growth exponent of 1/2. The flows spontaneously organize within fluid domains, exhibiting turbulent and chiral characteristics. Surprisingly, these turbulent flows can sustain hexatic order hydrodynamically stabilized by the Magnus force under certain conditions. Conversely, at higher speeds, nonlinear hydrodynamic interactions impede phase separation. Our findings illuminate the intriguing dynamic interplay between phase separation and chiral turbulence, effectively bridging the realms of phase ordering and turbulent physics.

DOI: 10.1103/PhysRevResearch.6.023186

I. INTRODUCTION

Phase separation is a fundamental phenomenon where an initially uniform system spontaneously separates into distinct phases, a process of significant importance in various domains, including the natural world [1,2], biology [3–5], and industrial applications [6,7]. Recently, there has been a renewed interest in phase separation, particularly due to its believed role in forming intracellular compartments such as nucleoli and stress granules [3,8]. In general, the phase-separation pattern in passive systems evolves to reduce the free-energy cost associated with the domain interface, a process called "domain coarsening." Typically, the pattern evolves following the power-law growth of the domain size $\langle \ell \rangle$ with time t as $\langle \ell \rangle \propto t^{\nu}$, where ν is the growth exponent. The values of ν depend on the specific mechanisms [1], such as evaporation-condensation [9,10] and the Brownian coagulation coarsening [11,12] characterized with $\nu = 1/3$ and Siggia's viscous hydrodynamics mechanism with $\nu = 1$ [1].

Although phase separation in systems solely composed of passive soft materials, including colloids [13–18] and polymers [7,19–21], has been studied extensively, recent attention has turned towards controlling domain coarsening [22–27] and pattern formation [28–35] by introducing active components. The presence of active particles in complex and crowded environments, even when intermixed with passive particles, has garnered significant interest, as emphasized in the comprehensive review by Bechinger *et al.* [36]. Particularly, active components influence the system by generating hydrodynamic interactions (HIs) as they move within the fluid medium [37–43], resulting in intricate many-body dynamic couplings among particles, a facet that has received relatively less attention. For example, Takatori *et al.* reported phase-separation experiments on a binary mixture of active actomyosin and passive lipid membrane [25]. Their findings demonstrated that the hydrodynamic flow generated by the active actomyosin yields an unusual coarsening exponent $\nu = 2/3$ of attractive lipid membranes [25], a twofold acceleration compared to the classical value of $\nu = 1/3$ [1]. Moreover, it has been shown that even a small quantity of self-propelled colloids can influence the self-assembly of passive colloids through HIs [31,34]. Active matter can also serve as a means to generate an effective long-range attraction between two parallel plates solely via HIs [43].

A notable category of active systems involves self-rotating particles generating vortical flows [44–52]. These particles are not only observed in biological systems [53–55] but are also engineered in experiments [48,49,52]. In experimental setups, the rotation speed (activity) of the rotors, such as magnetic rotors, can be precisely controlled by manipulating the frequency and amplitude of the applied magnetic field, enabling the creation of active turbulence [48]. Rotors in a fluid medium exhibit collective behaviors and self-organization primarily governed by HIs [46,51]. These behaviors range from dynamic hexatic ordering for rotors with single chirality [45,46] to the emergence of flowing bands

*tanaka@iis.u-tokyo.ac.jp

and rotating droplets for mixtures of rotors with opposite chiralities [45,51]. Recent work also demonstrated the ability to utilize chaotic turbulence to create distinct flow patterns trigger by the nonlinear effects of HI [56]. The authors have proposed a scenario in which rotation is initiated at the microscopic level through the rapid spinning of particles to attain sufficient inertia effects. Phase-separation dynamics and edge currents have been also explored in a system of rotating disks with short-range attractive interactions [57].

In this work, we employ the fluid particle dynamics (FPD) method [58,59] to investigate a two-dimensional (2D) binary mixture consisting of attractive colloids and active rotors immersed in a fluid. Strictly speaking, our active rotors should be termed "driven rotors," but we employ the term "active," as our results have implications for active matter. Through systematic adjustments of the area fraction of passive colloids, as well as the rotational speed and area fraction of active rotors, we reveal a diverse state diagram. This diagram encompasses branched clusters, spherical droplets, percolated networks, and nearly mixed states, all characterized by their dynamic fluctuations. Under specific conditions, we observe that attractive colloid domains exhibit power-law domain coarsening with a growth exponent of $\nu = 1/2$. This phenomenon is attributed to the inertial chiral flow generated by the active rotors. Interestingly, the characteristic inverse energy cascade of 2D turbulence is is bounded by the fluid domain size. We also observe an unconventional dynamically fluctuating arrested state caused by nonlinear hydrodynamic repulsions between rotating colloidal domains with the same chirality. Furthermore, we conducted simulations on quasi-2D colloidal monolayers confined between two plates. The results unequivocally demonstrate the relevance of our findings, derived from 2D simulations, for quasi-2D monolayers under strong confinement, thereby providing a foundation for experimental verification and further exploration of our system.

II. MODEL AND METHOD

Our model system comprises N_c attractive colloids and N_r active rotors in a solvent within a 2D periodic box of length L. Both colloids and rotors are modeled as fluid disks of viscosity η_p expressed as $\psi_i(\boldsymbol{r}) = \frac{1}{2}\{\tanh[(a - |\boldsymbol{r} - \boldsymbol{r}_i|)/\xi] + 1\}$, where a is the particle radius, ξ is the interface thickness, and $\boldsymbol{r}_i$ is the position vector of particle i. The particles interact via the shifted-truncated Lennard-Jones (LJ) potential with energy coupling ε and cutoff $r_{\rm cut}$. We set $r_{\rm cut} = 3\sigma$ for attractive colloid-colloid interaction and $r_{\rm cut} = 2^{1/6}\sigma$ for repulsive colloid-rotor and rotor-rotor interaction. To induce rotor rotation, we apply an external force $\boldsymbol{f}^i_T(\boldsymbol{r}) = \alpha|\boldsymbol{r} - \boldsymbol{r}_i|\psi_i(\boldsymbol{r})\boldsymbol{e}^i_\theta$ to each rotor, where $\alpha > 0$ is the strength of the torque and $\boldsymbol{e}^i_\theta$ is the unit vector perpendicular to $\boldsymbol{r} - \boldsymbol{r}_i$ in the counterclockwise direction [46,51].

We calculate the flow field $\boldsymbol{v}$ by using the FPD method [58,59], which directly solves the Navier-Stokes equation $\rho(\frac{\partial}{\partial t} + \boldsymbol{v}\cdot\nabla)\boldsymbol{v} = \boldsymbol{f} + \nabla\cdot(\boldsymbol{\sigma} + \boldsymbol{\sigma}^R)$, where ρ is the fluid density, $\boldsymbol{f}(\boldsymbol{r}) = \sum_i \boldsymbol{f}^i_{\rm LJ}\psi_i(\boldsymbol{r})/\int \psi_i(\boldsymbol{r}')d\boldsymbol{r}' + \sum_i \boldsymbol{f}^i_T$ is the force field, $\boldsymbol{f}^i_{\rm LJ}$ is the LJ force of particle i, and $\eta(\boldsymbol{r}) = \eta_s + (\eta_p - \eta_s)\sum_{i=1}\psi_i(\boldsymbol{r})$ is the viscosity field; $\boldsymbol{\sigma} = \eta(\boldsymbol{r})[\nabla\boldsymbol{v} + (\nabla\boldsymbol{v})^T] - p\boldsymbol{I}$ is the internal stress of the fluid, where $\boldsymbol{I}$ is the unit tensor and p is the pressure determined to satisfy the incompressible condition $\nabla\cdot\boldsymbol{v} = 0$. The position of particle i is updated by integrating the equation $d\boldsymbol{R}_i(t)/dt = \boldsymbol{V}_i(t)$, where $\boldsymbol{V}_i(t) = \int d^3\boldsymbol{r}[\boldsymbol{v}\psi_i(\boldsymbol{r})]$ is the particle velocity. By choosing $\eta_p = 50\eta_s$, we effectively suppress the flow within the particles, allowing us to approximate each particle as a rigid body [58,59]. The competition between the stirring flow of active rotors and the attraction between sticky colloids can be characterized by a dimensionless parameter $\gamma = \alpha\sigma^4/\varepsilon$. We set the length unit as the lattice size l_0, $a = 6.4l_0$, $\xi = l_0$, $\sigma = 2a + \xi$, and $\varepsilon = 100$, while systematically adjusting α to study the influence of active rotors. We use a system size $L = 2048l_0$, which is sufficiently large to avoid finite-size effects arising from the long-range nature of HIs. The time unit is chosen as $\tau_0 = \rho l_0^2/\eta_s$. We neglect thermal fluctuations, which is valid for deep quench conditions. This setting enables us to concentrate our investigation on the impact of HIs.

In quasi-2D simulations, we introduce flat walls at $z = 0$ and $z = h$, which are described by $\psi_{\rm wall} = \frac{1}{2}(\tanh\{[(L - h)/2 - |z - (L + h)/2|]/\xi\} + 1)$ with large viscosity $\eta_p = 50\eta_s$. The particles are confined in a monolayer and exhibit free movement within a plane at $z = 0.5\sigma$. This setup mimics an experimental situation, where colloidal particles dispersed in a liquid settle due to gravity on the bottom plate. Analogously to the 2D disk scenario, we exert an external force $\boldsymbol{f}^i_T(\boldsymbol{r}) = \alpha|(\boldsymbol{r} - \boldsymbol{r}_i)_\perp|\psi_i(\boldsymbol{r})\boldsymbol{e}^i_\theta$ to each 3D spherical rotor, where $\alpha > 0$ is the strength of the torque, $(\boldsymbol{r} - \boldsymbol{r}_i)_\perp$ is the vector component of $\boldsymbol{r} - \boldsymbol{r}_i$ perpendicular to the rotation axis $\boldsymbol{e}_z$ of the sphere, $\boldsymbol{e}_z$ is the unit vector in z dimension, and $\boldsymbol{e}^i_\theta$ is the unit vector perpendicular to $(\boldsymbol{r} - \boldsymbol{r}_i)_\perp$ and parallel to x-y plane in the counterclockwise direction. Due to computational constraints, we utilize a smaller box size $L = 256l_0$ and $a = 3.2l_0$ for quasi-2D simulations. We confirm that the incorporation of $\psi_{\rm wall}$ effectively suppresses the flow penetration into the upper and lower walls.

III. RESULTS AND DISCUSSION

A. Pattern formation and domain coarsening in a symmetric binary mixture

We first explore a symmetric binary mixture with colloids and rotors occupying an equal area fraction, $\phi_c = \phi_r = 0.15$. Figure 1 shows pattern evolution over time, t, for various α values. First, we observe that active rotors are entirely expelled from passive colloid domains into the fluid. Therefore, we may treat active rotors as part of the fluid phase. Notably, under $\alpha = 0.006$ [Fig. 1(a)], we observe an interconnected network structure, despite $\phi_c = 0.15$ being far below the percolation threshold $\phi_c^* \approx 0.22$ of the purely passive system [Fig. S1 in Ref. [60]]. This suggests that introducing slowly rotating particles reduces the percolation threshold for attractive colloids, enabling network formation even at low ϕ_c.

Increasing α from 0.03 to 0.12 [Figs. 1(b) and 1(c)] transforms the domain morphology of attractive colloids from dynamically fluctuating isolated branched clusters to round droplets rotating clockwise, opposing the rotor direction. This transformation in morphology is observable even in the very early stages of the phase-separation process. Interestingly, a similar transition between network and cluster patterns has

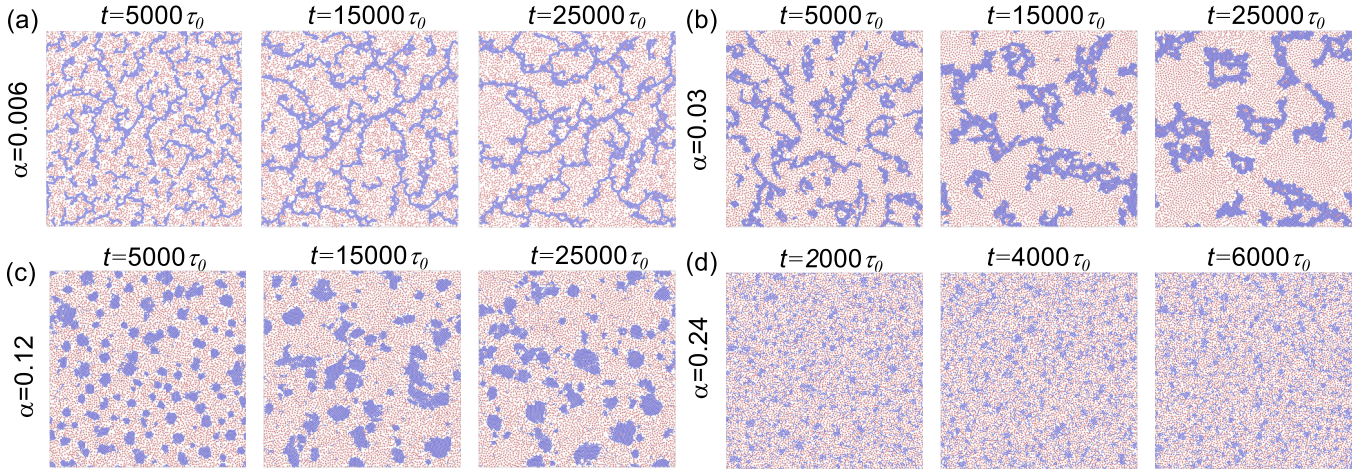

FIG. 1. Typical pattern formation and domain coarsening behaviors of a 2D binary mixture of colloidal particles (blue) and active rotors (red). Here both the area fraction of passive colloids, ϕ_c, and that of active rotors, ϕ_r, are set to 0.15. With increasing α, the phase-separation morphology of attractive colloids changes from (a) a percolated network structure ($\alpha = 0.006$) to (b) branched clusters ($\alpha = 0.03$), (c) round droplets ($\alpha = 0.12$), and (d) a nearly mixed state, where the domain coarsening is significantly suppressed ($\alpha = 0.24$). Unlike ordinary phase separation, these phase-separated structures undergo dynamic fluctuations induced by flows generated by rotors [refer to Supplemental movies S1–S4 in Supplemental Material (SM) [60], corresponding to (a)–(d)].

been reported for a mixture of sticky colloids and *Escherichia coli* bacteria [35]. However, in this system, the active agents produce a pusher-type flow pattern [61] in the linear hydrodynamic regime. Considering the differences in the flow pattern and the nonlinearity, the underlying mechanisms are expected to be fundamentally different.

The relationship between the radius of gyration R_g and the particle number n_c of each cluster indicates a fractal dimension d_f of approximately 1/2 for the case of $\alpha = 0.12$ [Fig. 2(b)]. In contrast, for $\alpha = 0.03$, d_f exceeds 1/2, particularly for larger aggregates [Fig. 2(a)], aligning with the observed patterns [Figs. 1(b) and 1(c)]. Further increasing α leads to an almost mixed state [Fig. 1(d)] at $\alpha = 0.24$. Strongly fluctuating flows suppress sharp interface formation and domain coarsening, resulting in fluctuating domains whose sizes are not significantly different from the particle size. This phenomenon can be explained by the competition between the stirring flow induced by the rotors and the attraction between sticky colloids, characterized by a dimensionless parameter $\gamma = \alpha\sigma^4/\varepsilon$. Although theoretical estimation is challenging due to many-body effects, our simulations suggest that when $\gamma \geqslant O(10^2)$, phase separation is nearly suppressed. These observations align with previous studies linking fluid turbulence to hindering domain growth [62–66]. Figure 1 also shows that in our system, pattern emergence is solely governed by HIs without the need for competing energetic interactions [67,68].

To quantify the domain coarsening, we calculate the characteristic wave number $\langle q \rangle$ for various α values [Fig. 3(a)], with $l = 2\pi/\langle q \rangle$ representing the characteristic domain size (see Ref. [60] for the definition of $\langle q \rangle$). Compared to the case without rotors, denoted as "wo" [black line in Fig. 3(a)], it is evident that the addition of rotors, which consistently generates hydrodynamic flow, notably enhances domain coarsening, except for $\alpha = 0.24$ [purple line in Fig. 3(a)]. The accelerated domain coarsening is responsible for the absence of network formation when augmenting α to $\alpha \geqslant 0.03$ since elongated chainlike structures in the early stage rapidly evolve into larger domains prior to percolating into a network.

Remarkably, $\langle q \rangle$ exhibits a power-law behavior $\langle q \rangle \sim t^{-1/2}$ for $\alpha = 0.03$, persisting for nearly a decade [blue line in Fig. 3(a)]. Conversely, for $\alpha = 0.06$ and 0.12, there is an initial transient period of $\langle q \rangle \sim t^{-1/2}$, followed by the dynamical arrest in the late stage [magenta and red lines in Fig. 3(a)], indicating a gradual approach to a steady state. The smaller

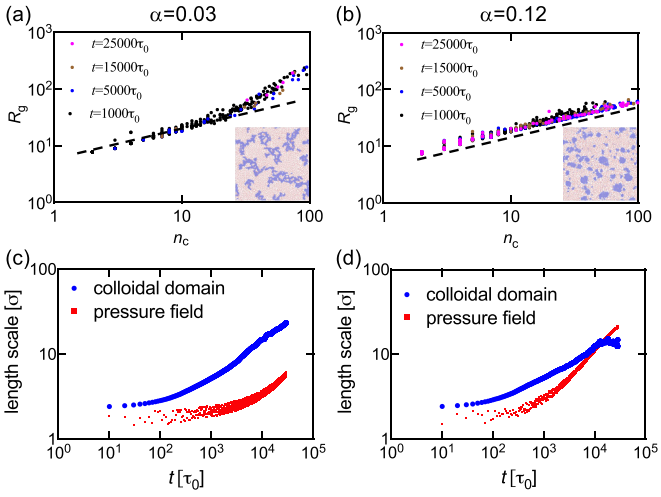

FIG. 2. Characterization of cluster shape and pressure inhomogeneity of a binary mixture ($\phi_c = 0.15$ and $\phi_r = 0.15$). (a) Relationship between the particle number n_c and the radius of gyration R_g of individual clusters for various times t. These results are obtained from simulations with $\alpha = 0.03$. (b) The same analysis as in panel (a) but for simulations with $\alpha = 0.12$. The dashed lines in (a) and (b) exhibit a slope of 1/2. (c) Temporal evolution of the chord length of colloid domains (blue curve; see Ref. [60] for chord length analysis) and the spatial correlation length of the pressure field (red curve; see main text for details) under $\alpha = 0.03$ in (c) and $\alpha = 0.12$ in (d).

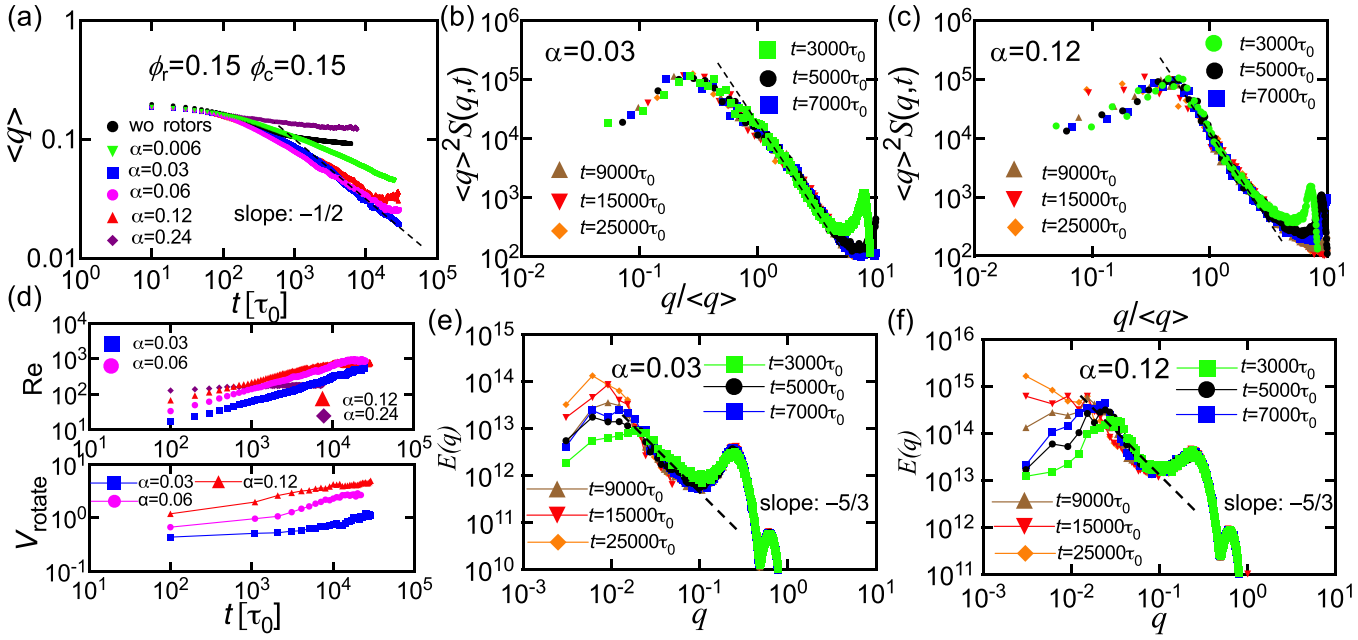

FIG. 3. Characterization of domain coarsening and the impact of inertial hydrodynamics on the phase-separation processes (at $\phi_c = \phi_r = 0.15$). (a) Temporal change of $\langle q \rangle$ for $\alpha = 0.006 \sim \alpha = 0.24$ as well as the case without rotors (denoted as "wo"). We find a power-law coarsening $\langle q \rangle \sim t^{-1/2}$ under $\alpha = 0.03$. The dashed line has a slope of $-1/2$. (b) Scaled structure factors $\langle q \rangle^d S(q,t)$ at different times as a function of $q/\langle q \rangle$ ($\alpha = 0.03$), which are collapsed on a single master curve, supporting the self-similar power-law domain coarsening. (c) Scaled structure factors $\langle q \rangle^d S(q,t)$ at different times as a function of $q/\langle q \rangle$ at $\alpha = 0.12$. These data cannot be collapsed onto a single master curve, particularly in the low-q region, indicating the breakdown of power-law growth. In (b) and (c), the dashed lines possess a slope of $-(d+1)$, which denotes the Porod law with the system dimension $d = 2$. (d) Top: Temporal change of the macroscopic-scale Reynolds number Re, determined from the flow velocity and the chord length of the fluid phase as the relevant velocity and length scale, respectively, for $\alpha = 0.03 \sim 0.24$. Bottom: Temporal change of the average rotational velocity $V_{\rm rotate}$ of individual clusters for $\alpha = 0.03 \sim \alpha = 0.12$. [(e) and (f)] The q dependence of the kinetic energy $E(q)$ for $\alpha = 0.03$ (e) and $\alpha = 0.12$ (f). We can see that the kinetic energy spectrum exhibits the characteristic form of $E(q) \sim q^{-5/3}$ within the intermediate q range, signifying the 2D turbulent nature of the hydrodynamic flow. Here the power-law regime is rather limited due to the small system size. The results for a larger system size are presented in Fig. S2 in Ref. [60], where the power-law regime spans a decade.

saturated domain size and the earlier onset of saturation for $\alpha = 0.12$ compared to $\alpha = 0.06$ indicate an increased level of inhibition of coarsening due to the stronger stirring flow generated by rotors.

In general, the self-similar nature of patterns underlies power-law domain coarsening [1]. Scaling wave number q with $\langle q \rangle$, we observe $\langle q \rangle^d S(q,t)$ at various times collapsing onto a single master curve for $\alpha = 0.03$ [Fig. 3(b); see Ref. [60] for $S(q,t)$ definition]. This self-similar domain growth supports power-law coarsening $\langle q \rangle \sim t^{-1/2}$. In contrast, for $\alpha = 0.12$, $\langle q \rangle^d S(q,t)$ at different times does not collapse on a single master curve in the late stage, consistent with the deviation from $\langle q \rangle \sim t^{-1/2}$ [Fig. 3(c)].

B. Hydrodynamic origin of active rotor-induced domain coarsening

Due to the athermal nature, the transport and coarsening of domains must involve a hydrodynamic origin. For phase separation in a binary fluid mixture with significant inertial effects, Furukawa predicted unconventional coarsening laws: $\langle q \rangle \sim t^{-2/(d+2)}$ for asymmetric composition and $\langle q \rangle \sim t^{-2/3}$ for symmetric composition [69]. We calculate the temporal change of the macroscopic-scale Reynolds number, Re, estimated from the average flow velocity v and chord length $\ell_{\rm out}$ [70] of the fluid domains with active rotors (see definition of $\ell_{\rm out}$ in Ref. [60]). We consistently observe a monotonic increase in Re over time, reaching approximately 10^2–10^3 after $t \approx 10^3 \tau_0$ [Fig. 3(d), top], despite the small particle-scale Re [$\sim O(10)$]. This phenomenon arises from the self-organization of flows confined within fluid domains, whose sizes increase over time.

We compute the kinetic energy spectrum $E(q)$ [Figs. 3(e) and 3(f); see Ref. [60] for the definition of $E(q)$], identifying a q regime where $E(q) \sim q^{-5/3}$, a fundamental characteristic of 2D turbulence [71]. We confirm that this power law persists for a decade in a larger simulation system ($L = 4096 l_0$ and $\alpha = 0.03$), further supporting 2D turbulent flow (Fig. S2 in Ref. [60]). Furthermore, we observe kinetic energy transfer from the small rotor scale where energy is input [as evidenced by the second peak in $E(q)$] to the larger fluid-domain scale, supported by the shift of the first peak in $E(q)$, indicating an inverse energy cascade typical of 2D turbulence. The confinement of turbulent flow by the colloid-rich phase accounts for the lower q bound of the power law. Collectively, these findings suggest that rotating particles induce turbulent, inertial hydrodynamic flow governing domain growth, resulting in $\langle q \rangle \sim t^{-1/2}$ [for $\alpha = 0.03$; Fig. 3(a)]. This supports that this growth exponent originates from 2D turbulent flow generated by rotors.

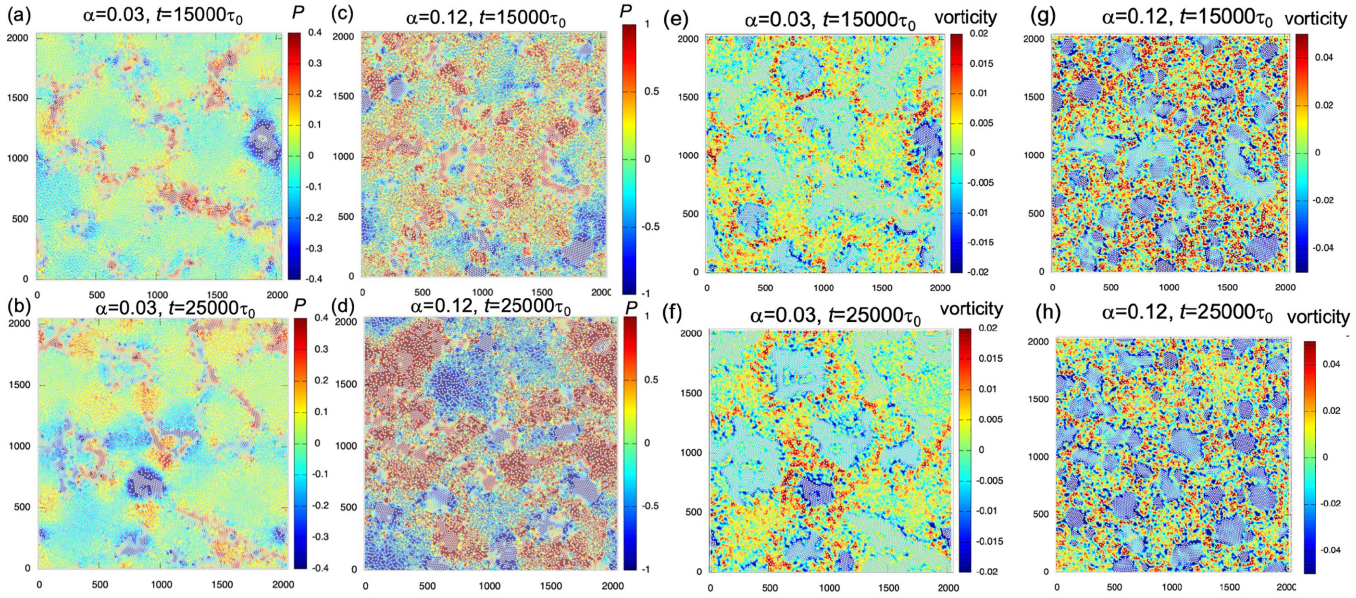

FIG. 4. Visualization of the pressure field P in a mixture ($\phi_c = \phi_r = 0.15$) at $t = 15\,000\tau_0$ and $t = 25\,000\tau_0$ for [(a) and (b)] $\alpha = 0.03$ and [(c) and (d)] $\alpha = 0.12$. The color represents the value of the local pressure (see the color bars), maintaining the incompressible condition $\nabla \cdot \boldsymbol{v} = 0$. Particles are displayed with a semitransparent overlay atop the pressure map. We find that the pressure field of the solvent exhibits significant spatial inhomogeneity. This inhomogeneity is linked with the transport of isolated clusters and the resulting domain coarsening. For $\alpha = 0.12$ (d), the typical size of a high-pressure region far exceeds the domain size of isolated droplets at the late stage ($t = 25\,000\tau_0$), manifesting a slowdown of the coarsening process. Visualization of the flow-field vorticity ω, defined as $\omega = \nabla \times \boldsymbol{v}$, where $\boldsymbol{v} = (v_x, v_y)$ represents the velocity field, for cases [(e) and (f)] with $\alpha = 0.03$ and [(g) and (h)] with $\alpha = 0.12$. Here we employ a coarse-grained velocity field at a length resolution of $16l_0$. It is observed that rotors and colloid domains exhibit vorticity with opposite signs, suggesting that the turbulent flow generated in our system possesses chiralities rather than being structureless in the conventional sense.

For $\alpha = 0.12$, after a period of power-law growth ($\langle q \rangle \sim t^{-1/2}$), the system eventually experiences dynamical arrest with slowed domain coarsening [Fig. 3(a)], despite the relatively high macroscopic-scale Re [Fig. 3(d), top]. The rotational speed of droplet domains is notably higher for $\alpha = 0.06$ and $\alpha = 0.12$, reaching a plateau in the late stage [Fig. 3(d), bottom]. A similar dynamic arrest of domain coarsening has been documented in symmetric binary fluid mixtures subjected to 2D achiral turbulence in the absence of active particles [72].

The motion of colloidal clusters and active rotors generates a large-scale flow with a strongly inhomogeneous pressure field (Figs. 4(a)–4(d); also see Fig. S3 in Ref. [60]). The characteristic length scale of the pressure field expands as domain coarsening progresses. Comparing the pressure field under $\alpha = 0.03$ [Figs. 4(a) and 4(b)] with $\alpha = 0.12$ [Figs. 4(c) and 4(d)], we observe a significant increase in the characteristic length scale of high-pressure domains with α, especially in the late stage [$t = 25\,000\tau_0$; Fig. 4(d)]. To quantify this phenomenon, we calculate the spatial correlation of the pressure field, defined as $f_P(r) = \langle P(0)P(r)\rangle / \langle P(0)^2\rangle$, and determine the correlation length as the distance at which f_P decreases to a threshold of e^{-1}. Interestingly, for $\alpha = 0.03$, we observe that the characteristic length scale of the pressure field coherently increases with the domain size [Fig. 2(c)]. However, when α is elevated to $\alpha = 0.12$, the characteristic length scale of pressure domains develops rapidly and eventually surpasses the cluster size in the late stages [Fig. 2(d)]. Notably, this crossover occurs at the timing when phase separation is hindered and deviates from $\langle q \rangle \sim t^{-1/2}$ [see the red line in Fig. 3(a)]. These results collectively indicate that momentum transport occurs at a length scale much greater than the colloidal droplet size. More specifically, the strong repulsion of rapidly spinning rotors from the repulsive Magnus force [46] prevents colloidal droplet coagulation, ultimately leading to a deviation from power-law growth. This can be also seen from the velocity field (Fig. S4 in Ref. [60]) where rotors tend to maintain distance due to the repulsive Magnus force generated

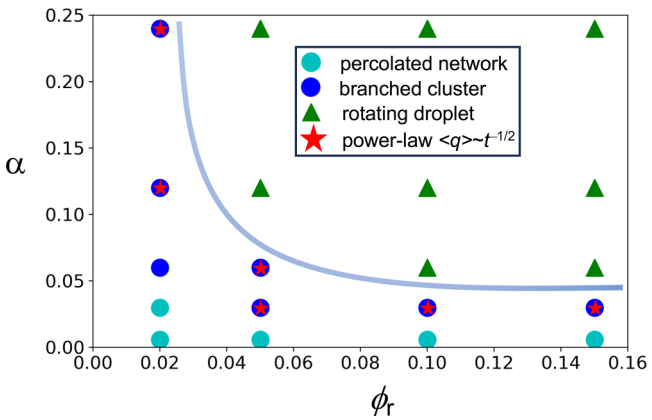

FIG. 5. The general state diagram on the ϕ_r-α plane, with $\phi_c = 0.15$. For each value of ϕ_r, we observe a pattern selection, transitioning from a percolated network to branched clusters and finally to rotating round droplets with increasing α. The red stars indicate state points where we observe power-law coarsening behavior of $\langle q \rangle \sim t^{-1/2}$ [69].

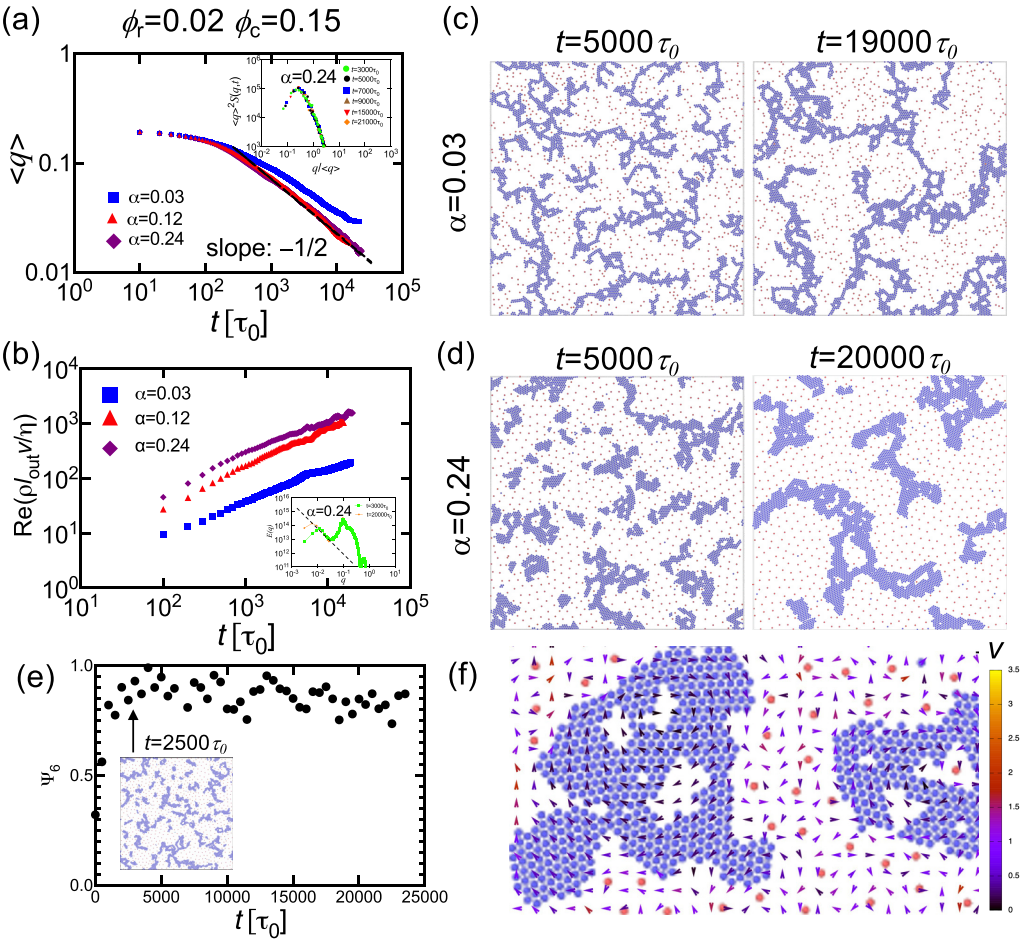

FIG. 6. Pattern formation and domain coarsening of a binary mixture ($\phi_c = 0.15$ and $\phi_r = 0.02$). (a) Temporal change of $\langle q \rangle$ for $\alpha = 0.03$, $\alpha = 0.12$, and $\alpha = 0.24$. The dashed line represents a power law with $\nu = 1/2$. The inset shows the scaled structure factors $\langle q \rangle^d S(q,t)$, which are collapse onto a single master curve, supporting power-law domain coarsening under $\alpha = 0.24$ (also $\alpha = 0.12$; data not shown). (b) Temporal change of the macroscopic-scale Reynolds number Re for $\alpha = 0.03$, $\alpha = 0.12$, and $\alpha = 0.24$. The inset shows the q dependence of the kinetic energy spectrum $E(q)$ for $\alpha = 0.24$ where the dashed line has a slope of $-5/3$. [(c) and (d)] Pattern evolution as a function of time t for (c) $\alpha = 0.03$ and (d) $\alpha = 0.24$. In (d), we observe that rotors self-organize into hexagonal arrangements. See Supplemental movie S5 in SM [60] for the phase-separation behavior illustrated in (d). (e) The temporal evolution of the hexagonal order parameter ψ_6 at $\alpha = 0.24$. It reveals the emergence of hexagonal order within the rotor phase, evident even as early as $t = 2500\tau_0$. Subsequently, ψ_6 maintains a consistently high value despite the dynamical motion of the rotors. (f) The flow velocity field $(\boldsymbol{v}_x, \boldsymbol{v}_y)$ within a specified region at $\alpha = 0.24$, showcasing an edge flow pattern along the colloid domain boundary. Here we present a coarse-grained velocity field characterized by a length resolution of $24l_0$.

by the local pressure difference between the rotating side and the opposite side, reducing droplet coarsening tendency. We also note that HIs induce an effective attraction between rotating disks, as discussed in Ref. [46]. However, the repulsive Magnus interaction prevails over this effective attraction for a high area fraction of rotating particles [46,51], making it not relevant in this situation.

Additionally, we analyze the flow-field vorticity for $\alpha = 0.03$ [Figs. 4(e) and 4(f)] and $\alpha = 0.12$ [Figs. 4(g) and 4(h)] and observe that rotors and colloid domains exhibit vorticity with opposite signs. These results correspond to their respective counterclockwise and clockwise rotations, confirming the presence of large-scale chiralities within the turbulent flow generated in our systems.

We note that, in a rotor-only system, the static state features hexatic ordering and a uniform pressure field [46]. The nonuniform pressure field in Fig. 4 results from complex couplings between active rotors and passive attractive colloids. For large α, dynamical couplings between rotors and colloids lead to the self-organization of large-scale vortex flow [Figs. 4(g) and 4(h)], characterized by large pressure domains with high and low pressures [Figs. 4(c) and 4(d)]. This aligns with the slowing down of coarsening dynamics in later stages, as neighboring colloidal droplets within the same pressure domain cannot coalesce to form larger droplets.

Accordingly, increasing α has a dual impact on coarsening. Higher α induces inertial hydrodynamic flow, leading to domain transport, but it also results in substantial nonlinear hydrodynamic repulsion between domains, especially for round rotating droplets. This enhanced repulsion causes dynamic arrest, leading to a deviation from power-law coarsening in the late stage. For $\alpha = 0.24$, the macroscopic-scale

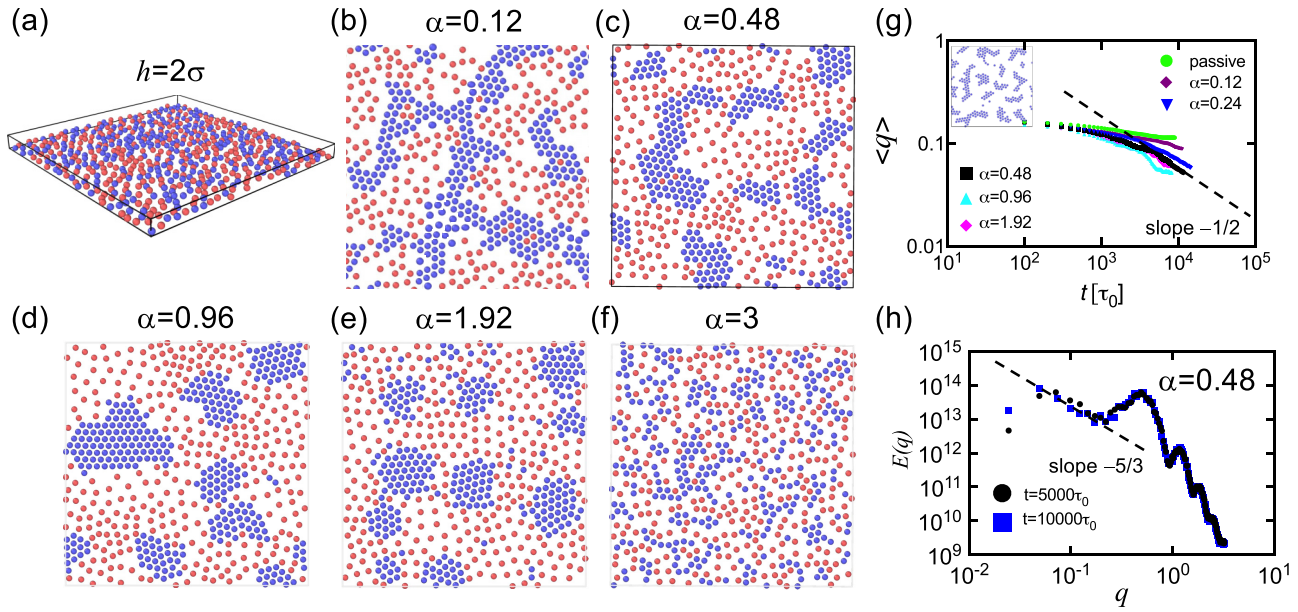

FIG. 7. Phase-separation dynamics of a quasi-2D monolayer of colloidal particles and active rotors ($\phi_c = \phi_r = 0.15$) confined in a slab geometry. (a) The initial random configuration of a 2D binary mixture of colloidal particles (blue) and active rotors (red). The thickness of the slab is $h = 2\sigma$ (σ: particle diameter), and particles' centers of mass can move freely on a plane at $z = 0.5\sigma$. [(b)–(f)] Typical pattern formation of a 2D binary mixture. Here both the area fraction of passive colloids, ϕ_c, and that of active rotors, ϕ_r, are set to 0.15. As the parameter α is elevated, the phase-separation morphology of colloidal particles changes from (b) a percolated network and (c) elongated branched clusters to [(d) and (e)] round droplets, ultimately leading to (f) a nearly mixed state. The observed transition patterns are essentially the same as those identified in a 2D system (Fig. 1). (g) Temporal change of $\langle q \rangle$ for $\alpha = 0.12 \sim \alpha = 1.92$ as well as the case of purely passive colloids without rotors. We find a power-law coarsening $\langle q \rangle \sim t^{-1/2}$ under the intermediate $\alpha = 0.24$ and $\alpha = 0.48$. The dashed line has a slope of $-1/2$. (h) The q dependence of the kinetic energy $E(q)$ for $\alpha = 0.48$ at different times t during the power-law coarsening regime. The kinetic energy spectrum illustrates the transfer of energy from the small rotor scale, where energy is input, to large-scale fluid domains. This transfer is characterized by $E(q) \sim q^{-5/3}$ in the intermediate q range, a hallmark of 2D turbulence, albeit with a narrow power-law range. These results confirm that the conclusions drawn from 2D simulations hold true for a quasi-2D monolayer system under sufficiently strong confinement ($h = 2\sigma$).

Reynolds number Re does not evolve with time and remains constant [Fig. 3(d), top], indicating the disappearance of large-scale coherent flow development, consistent with the small domain scale [Fig. 3(a)].

C. Extension to asymmetric binary mixture and general dynamic state diagram

To examine the generality of our findings, we also investigate asymmetric binary mixtures, varying the ratios of the area fraction between passive colloids (ϕ_c) and active rotors (ϕ_r). In Fig. 5, we present the state diagram on the ϕ_r-α plane, maintaining $\phi_c = 0.15$. We observe that the pattern selection between percolated networks, branched clusters, and rotating droplets persists for different values of $\phi_r < \phi_c = 0.15$. Near the state boundary (marked with red stars), we consistently note power-law domain coarsening behavior (see Figs. S5 and S6 in Ref. [60] for detailed $\langle q \rangle$ at $\phi_r = 0.1$ and $\phi_r = 0.05$ and Fig. 6 for $\phi_r = 0.02$).

Interestingly, for $\phi_r = 0.02$ and $\alpha = 0.12 \sim 0.24$, rotors self-organize into hexagonal arrangements [Fig. 6(d)] in the rotor-rich fluid phase, characterized by the hexagonal order parameter $\psi_6 \approx 1$ [Fig. 6(e); see Ref. [60] for the definition of ψ_6], reminiscent of systems of pure rotors [46]. This hexagonal arrangement of active rotors likely results from reduced spatial confinement of rotors at small ϕ_r values, enabling hexatic ordering via nonlinear hydrodynamic repulsions due to Magnus effects [46]. The flow velocity field at $\alpha = 0.24$ also exhbits an edge flow pattern along the colloid domain boundary [Fig. 6(f)], resulting in the rotation of the colloid domains (See Supplemental movie S5 in SM [60]).

Remarkably, nonlinear hydrodynamics enables the coexistence of power-law self-similar growth of passive colloid domains and hexatic ordering of active rotors in this case ($\phi_r = 0.02$ and $\alpha = 0.24$). In the inset of Fig. 6(b), it is illustrated that the inverse energy cascade takes place in the fluid domains exhibiting hexatic order. This observation suggests an exotic dynamic coexistence between turbulence and static spatial order, both of which originate from nonlinear hydrodynamics. Additionally, these findings suggest the presence of a parameter space region, characterized by Re $\approx 10^2$–10^3, where power-law coarsening ($\langle q \rangle \sim t^{-1/2}$) is observed. Overall, Fig. 5 confirms that pattern selection, driven by varying α, is a general phenomenon.

Increasing the colloidal area fraction to $\phi_c = 0.3$, exceeding $\phi_c^* \approx 0.22$, transforms the pattern from a percolated network to round droplets as α increases (Figs. S7(a) and S7(b) in Ref. [60]). In all cases, we observe slowed domain evolution in the late stage without achieving power-law coarsening (Fig. S7(c) in Ref. [60]). Notably, even in the late stage, Re becomes much smaller at $\phi_c = 0.3$, reaching Re $\lesssim 10^2$ (Fig. S7(d) in Ref. [60]).

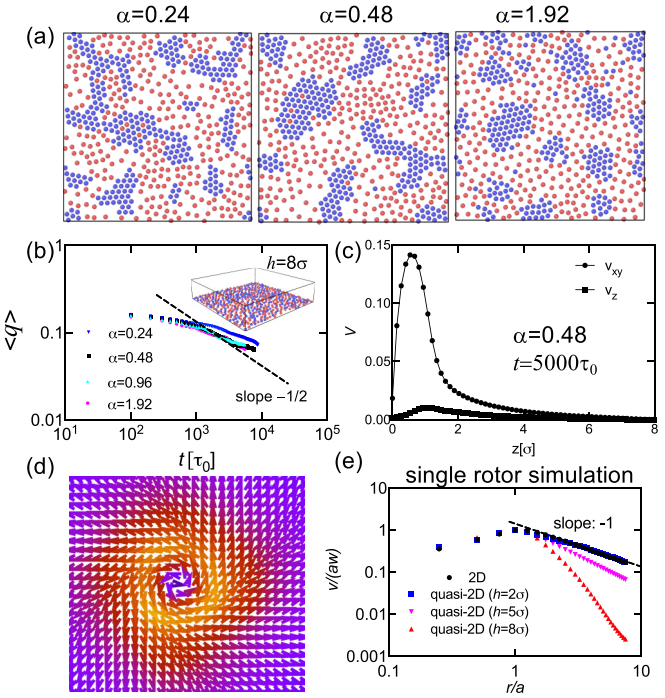

FIG. 8. Phase-separation processes of a quasi-2D monolayer of colloidal particles and active spherical rotors ($\phi_c = \phi_r = 0.15$) confined in a slab. The thickness of the slab is $h = 8\sigma$ (σ: particle diameter), and particles' centers of mass can move freely on a plane at $z = 0.5\sigma$. (a) Typical pattern formation of elongated branched clusters and round droplets under $\alpha = 0.24$, $\alpha = 0.48$, and $\alpha = 1.92$. (b) Temporal change of $\langle q \rangle$ for different settings of α. The inset shows the initial random configuration of a quasi-2D binary mixture of colloidal particles (blue) and active rotors (red). (c) The average flow velocity magnitudes, denoted as v_{xy} (in the $x - y$ dimension) and v_z (in the z dimension), plotted against the height z. We observe a greater intensity of flow velocity in the $x - y$ plane compared to the flow-field velocity in the z dimension. Moreover, the flow field exhibits a gradual decay in the distant region from the monolayer until the upper wall at $z = h = 8\sigma$. Here we show the flow field under $\alpha = 0.48$ at time $t = 5000\tau_0$. The observed patterns closely resemble those observed under stronger confinement with $h = 2\sigma$, as shown in Fig. 7. However, we do not observe the power-law behavior of $\langle q \rangle \sim t^{-1/2}$ for intermediate α, unlike in the cases of $h = 0$ and 2σ (Fig. 7), highlighting the influence of the additional z dimension in facilitating the flow's escape. (d) The rotating flow pattern around a single active rotor for $h = 8\sigma$. (e) The flow-field velocity $v/(a\omega)$ in relation to r/a, where r is the distance to the center, ω is the angular frequency, and (a) is the radius. The flow velocity decays as $1/r$ outside the particle, which is a characteristic feature of a 2D rotating disk, known as "Rankin vortex" [46]. This feature consistently remains for $h = 2\sigma$ but is absent for $h = 8\sigma$, indicating deviations from 2D hydrodynamics. The dashed line has a slope of -1.

D. Applicability to quasi-2D colloidal monolayers

Finally, we explore the applicability of our findings in pure 2D systems for more realistic quasi-2D monolayers confined between two flat substrates. We confirm the validity of our findings for strong confinement (interplate separation $h = 2\sigma$; see Fig. 7). Note that the flow velocity is zero at the walls, thus corresponding to no-slip boundary conditions (Fig. S8 in Ref. [60]). For weaker confinement (e.g., $h = 8\sigma$), the domain patterns [Fig. 8(a)] still closely resemble those for $h = 2\sigma$. However, unlike in 2D [Fig. 3(a)] and strongly confined quasi-2D systems (Fig. 7), there is no power-law coarsening $\langle q \rangle \sim t^{-1/2}$ observed for intermediate α, as depicted in Fig. 8(b). These results indicate the non-negligible influence of the extra dimension in facilitating flow's escape [Fig. 8(c)] is responsible for a departure from 2D hydrodynamics [46,69]. In fact, even at the single rotor level, as the separation between the wall gradually increases, we observe a much faster decay of the flow field surrounding a rotor [Figs. 8(d) and 8(e)]. This observation highlights the significant influence of the confinement effect in causing deviations from 2D hydrodynamics.

IV. CONCLUSIONS

In summary, we have investigated the pattern formation and domain coarsening in a binary mixture of attractive colloids and self-rotating particles by accounting for the many-body hydrodynamic interactions through FPD method [58,59]. We have demonstrated that hydrodynamic interactions can induce various phase-separation morphologies, including percolated networks, branched clusters, round droplets, and nearly mixed states, in a binary mixture of attractive colloids and active rotors in a solvent. Precise control over domain shape and coarsening kinetics is achievable by adjusting rotor area fraction and rotational speed.

Notably, the coarsening of colloidal particle domains exhibits self-similar, power-law growth with an exponent of $\nu = 1/2$ under intermediate rotational speeds, attributed to the inertial chiral hydrodynamic flow generated by active rotors. Additionally, under certain conditions, nonlinear hydrodynamics surprisingly facilitates the coexistence of self-similar, power-law growth of passive colloid domains, and hexatic ordering of active rotors in the fluid phase. We have also identified an unconventional mechanism of dynamic arrest induced by nonlinear hydrodynamic repulsions between rotating colloid domains when the activity of rotors is enhanced. This phenomenon is unique to turbulence exhibiting chiral symmetry breaking.

These findings collectively deepen our understanding of the intricate dynamics observed in mixture systems of passive colloids and active rotors. Furthermore, we performed hydrodynamic simulations of quasi-2D monolayers constrained between two plates, a setup frequently used in experimental settings. Our findings unequivocally confirm the applicability of our results, mainly obtained from 2D simulations, to quasi-2D monolayers under sufficiently strong confinement. This sets the stage for experimental validation and further exploration of our system.

Ordinary phase separation of passive soft materials in the inertial hydrodynamic regime is seldom explored because it only becomes relevant in the very late stages of domain coarsening. For example, Kendon *et al.* [73,74] studied the spinodal decomposition of a 3D symmetric binary fluid using lattice-Boltzmann simulations and successfully replicated Furukawa's prediction, $\langle q \rangle \sim t^{-2/3}$ [69]. Due to its extensive computational demands, particle-based simulations have not tackled the inertial growth regime. One potential approach to

achieve the inertial hydrodynamic regime involves turbulent stirring of the fluid, explored in both experiments [62,64] and simulations [65,66,75]. It has been observed that domain coarsening is arrested after intense stirring, where power-law growth has not been observed. Our system induces inertial chiral hydrodynamic flow through fast-rotating particles, leading to intriguing pattern selection and the replication of Furukawa's inertial growth law, $\langle q \rangle \sim t^{-1/2}$ [69], albeit with the addition of chirality, particularly for intermediate rotational speeds. Interestingly, we observe that this phenomenon is accompanied by an inverse energy cascade characteristic of 2D turbulence, constrained by the fluid domain size.

Simulating soft and active matter under the many-body HIs poses a significant challenge. Our work offers guidance for leveraging the hydrodynamic flow created by rotating particles to drive phase separation and pattern formation in passive materials. This facilitates further exploration into the dynamics of nonequilibrium phase ordering in the nonlinear inertial hydrodynamic regime, effectively connecting the domains of phase ordering and turbulent physics.

ACKNOWLEDGMENTS

This work was supported by the Grants-in-Aid for Specially Promoted Research (JSPS KAKENHI Grant No. JP20H05619) from the Japan Society for the Promotion of Science (JSPS). The authors acknowledge the Information Technology Center and the Institute for Solid State Physics at the University of Tokyo for providing computational resources.

[1] A. Onuki, *Phase Transition Dynamics* (Cambridge University Press, Cambridge, UK, 2002).
[2] M. Doi, *Soft Matter Physics* (Oxford University Press, Oxford, 2013).
[3] C. P. Brangwynne, C. R. Eckmann, D. S. Courson, A. Rybarska, C. Hoege, J. Gharakhani, F. Jülicher, and A. A. Hyman, Germline P granules are liquid droplets that localize by controlled dissolution/condensation, Science **324**, 1729 (2009).
[4] P. Li, S. Banjade, H.-C. Cheng, S. Kim, B. Chen, L. Guo, M. Llaguno, J. V. Hollingsworth, D. S. King, S. F. Banani *et al.*, Phase transitions in the assembly of multivalent signalling proteins, Nature (London) **483**, 336 (2012).
[5] S. Alberti, A. Gladfelter, and T. Mittag, Considerations and challenges in studying liquid-liquid phase separation and biomolecular condensates, Cell **176**, 419 (2019).
[6] C. Gallegos and J. M. Franco, Rheology of food, cosmetics and pharmaceuticals, Curr. Opin. Colloid Interface Sci. **4**, 288 (1999).
[7] F. Wang, P. Altschuh, L. Ratke, H. Zhang, M. Selzer, and B. Nestler, Progress report on phase separation in polymer solutions, Adv. Mater. **31**, 1806733 (2019).
[8] A. A. Hyman, C. A. Weber, and F. Jülicher, Liquid-liquid phase separation in biology, Annu. Rev. Cell Dev. Biol. **30**, 39 (2014).
[9] I. M. Lifshitz and V. V. Slyozov, The kinetics of precipitation from supersaturated solid solutions, J. Phys. Chem. Solids **19**, 35 (1961).
[10] C. Wagner, Theory of precipitate change by redissolution, Z. Elektrochem **65**, 581 (1961).
[11] M. Smoluchowski, Drei vortrage uber diffusion, brownsche bewegung und koagulation von kolloidteilchen, Z. Phys. **17**, 557 (1916).
[12] R. Shimizu and H. Tanaka, A novel coarsening mechanism of droplets in immiscible fluid mixtures, Nat. Commun. **6**, 7407 (2015).
[13] H. Tanaka, Y. Nishikawa, and T. Koyama, Network-forming phase separation of colloidal suspensions, J. Phys.: Condens. Matter **17**, L143 (2005).
[14] A. E. Bailey, W. C. K. Poon, R. J. Christianson, A. B. Schofield, U. Gasser, V. Prasad, S. Manley, P. N. Segre, L. Cipelletti, W. V. Meyer, M. P. Doherty, S. Sankaran, A. L. Jankovsky, W. L. Shiley, J. P. Bowen, J. C. Eggers, C. Kurta, T. Lorik, P. N. Pusey, and D. A. Weitz, Spinodal decomposition in a model colloid-polymer mixture in microgravity, Phys. Rev. Lett. **99**, 205701 (2007).
[15] A. Furukawa and H. Tanaka, Key role of hydrodynamic interactions in colloidal gelation, Phys. Rev. Lett. **104**, 245702 (2010).
[16] G. Foffi, C. De Michele, F. Sciortino, and P. Tartaglia, Arrested phase separation in a short-ranged attractive colloidal system: A numerical study, J. Chem. Phys. **122**, 224903 (2005).
[17] M. Tateno and H. Tanaka, Numerical prediction of colloidal phase separation by direct computation of Navier–Stokes equation, npj Comput. Mater. **5**, 40 (2019).
[18] M. Tateno and H. Tanaka, Power-law coarsening in network-forming phase separation governed by mechanical relaxation, Nat. Commun. **12**, 912 (2021).
[19] H. Tanaka, Unusual phase separation in a polymer solution caused by asymmetric molecular dynamics, Phys. Rev. Lett. **71**, 3158 (1993).
[20] A. Bhattacharya, S. D. Mahanti, and A. Chakrabarti, Network-like pattern formation in phase separating polymer solutions: A molecular dynamics study, Phys. Rev. Lett. **80**, 333 (1998).
[21] J. Yuan, M. Tateno, and H. Tanaka, Mechanical slowing down of network-forming phase separation of polymer solutions, ACS Nano **17**, 18025 (2023).
[22] J. Stenhammar, R. Wittkowski, D. Marenduzzo, and M. E. Cates, Activity-induced phase separation and self-assembly in mixtures of active and passive particles, Phys. Rev. Lett. **114**, 018301 (2015).
[23] J. Smrek and K. Kremer, Small activity differences drive phase separation in active-passive polymer mixtures, Phys. Rev. Lett. **118**, 098002 (2017).
[24] J. L. Aragones, J. P. Steimel, and A. Alexander-Katz, Aggregation dynamics of active rotating particles in dense passive media, Soft Matter **15**, 3929 (2019).
[25] D. P. Arnold, A. Gubbala, and S. C. Takatori, Active surface flows accelerate the coarsening of lipid membrane domains, Phys. Rev. Lett. **131**, 128402 (2023).
[26] S. Dikshit and S. Mishra, Activity-driven phase separation and ordering kinetics of passive particles, Eur. Phys. J. E **45**, 21 (2022).
[27] S. Bhattacharyya and J. M. Yeomans, Phase separation driven by active flows, Phys. Rev. Lett. **130**, 238201 (2023).

[28] R. Ni, M. A. Cohen Stuart, and P. G. Bolhuis, Tunable long range forces mediated by self-propelled colloidal hard spheres, Phys. Rev. Lett. **114**, 018302 (2015).
[29] C. Reichhardt and C. J. O. Reichhardt, Reversibility, pattern formation, and edge transport in active chiral and passive disk mixtures, J. Chem. Phys. **150**, 064905 (2019).
[30] Z. Ma, M. Yang, and R. Ni, Dynamic assembly of active colloids: Theory and simulation, Adv. Theory Simul. **3**, 2000021 (2020).
[31] H. R. Vutukuri, M. Lisicki, E. Lauga, and J. Vermant, Light-switchable propulsion of active particles with reversible interactions, Nat. Commun. **11**, 2628 (2020).
[32] A. V. Singh, V. Kishore, G. Santomauro, O. Yasa, J. Bill, and M. Sitti, Mechanical coupling of puller and pusher active microswimmers influences motility, Langmuir **36**, 5435 (2020).
[33] S. M. Mousavi, G. Gompper, and R. G. Winkler, Active bath-induced localization and collapse of passive semiflexible polymers, J. Chem. Phys. **155**, 044902 (2021).
[34] I. P. Madden, L. Wang, J. Simmchen, and E. Luijten, Hydrodynamically controlled self-organization in mixtures of active and passive colloids, Small **18**, 2107023 (2022).
[35] D. Grober, I. Palaia, M. C. Uçar, E. Hannezo, A. Šarić, and J. Palacci, Unconventional colloidal aggregation in chiral bacterial baths, Nat. Phys. **19**, 1680 (2023).
[36] C. Bechinger, R. Di Leonardo, H. Löwen, C. Reichhardt, G. Volpe, and G. Volpe, Active particles in complex and crowded environments, Rev. Mod. Phys. **88**, 045006 (2016).
[37] J. M. Yeomans, D. O. Pushkin, and H. Shum, An introduction to the hydrodynamics of swimming microorganisms, Eur. Phys. J. Spec. Top. **223**, 1771 (2014).
[38] M. Theers, E. Westphal, K. Qi, R. G. Winkler, and G. Gompper, Clustering of microswimmers: interplay of shape and hydrodynamics, Soft Matter **14**, 8590 (2018).
[39] R. Singh and M. E. Cates, Hydrodynamically interrupted droplet growth in scalar active matter, Phys. Rev. Lett. **123**, 148005 (2019).
[40] S. Yang, M. Huang, Y. Zhao, and H. P. Zhang, Controlling cell motion and microscale flow with polarized light fields, Phys. Rev. Lett. **126**, 058001 (2021).
[41] M. R. Shaebani, A. Wysocki, R. G. Winkler, G. Gompper, and H. Rieger, Computational models for active matter, Nat. Rev. Phys. **2**, 181 (2020).
[42] J. Yuan, K. Takae, and H. Tanaka, Impact of inverse squeezing flow on the self-assembly of oppositely charged colloidal particles under electric field, Phys. Rev. Lett. **129**, 248001 (2022).
[43] L. Ning, X. Lou, Q. Ma, Y. Yang, N. Luo, K. Chen, F. Meng, X. Zhou, M. Yang, and Y. Peng, Hydrodynamics-induced long-range attraction between plates in bacterial suspensions, Phys. Rev. Lett. **131**, 158301 (2023).
[44] N. H. Nguyen, D. Klotsa, M. Engel, and S. C. Glotzer, Emergent collective phenomena in a mixture of hard shapes through active rotation, Phys. Rev. Lett. **112**, 075701 (2014).
[45] K. Yeo, E. Lushi, and P. M. Vlahovska, Collective dynamics in a binary mixture of hydrodynamically coupled microrotors, Phys. Rev. Lett. **114**, 188301 (2015).
[46] Y. Goto and H. Tanaka, Purely hydrodynamic ordering of rotating disks at a finite reynolds number, Nat. Commun. **6**, 5994 (2015).
[47] K. Yeo, E. Lushi, and P. M. Vlahovska, Dynamics of inert spheres in active suspensions of micro-rotors, Soft Matter **12**, 5645 (2016).
[48] G. Kokot, S. Das, R. G. Winkler, G. Gompper, I. S. Aranson, and A. Snezhko, Active turbulence in a gas of self-assembled spinners, Proc. Natl. Acad. Sci. USA **114**, 12870 (2017).
[49] Y. Wang, S. Canic, G. Kokot, A. Snezhko, and I. S. Aranson, Quantifying hydrodynamic collective states of magnetic colloidal spinners and rollers, Phys. Rev. Fluids **4**, 013701 (2019).
[50] Z. Shen and J. S. Lintuvuori, Hydrodynamic clustering and emergent phase separation of spherical spinners, Phys. Rev. Res. **2**, 013358 (2020).
[51] B. Hrishikesh, K. Takae, E. Mani, and H. Tanaka, Phase separation of rotor mixtures without domain coarsening driven by two-dimensional turbulence, Commun. Phys. **5**, 337 (2022).
[52] A. Modin, M. Y. Ben Zion, and P. M. Chaikin, Hydrodynamic spin-orbit coupling in asynchronous optically driven microrotors, Nat. Commun. **14**, 4114 (2023).
[53] I. H. Riedel, K. Kruse, and J. Howard, A self-organized vortex array of hydrodynamically entrained sperm cells, Science **309**, 300 (2005).
[54] K. Drescher, K. C. Leptos, I. Tuval, T. Ishikawa, T. J. Pedley, and R. E. Goldstein, Dancing volvox: Hydrodynamic bound states of swimming algae, Phys. Rev. Lett. **102**, 168101 (2009).
[55] A. P. Petroff, X.-L. Wu, and A. Libchaber, Fast-moving bacteria self-organize into active two-dimensional crystals of rotating cells, Phys. Rev. Lett. **114**, 158102 (2015).
[56] X. M. de Wit, M. Fruchart, T. Khain, F. Toschi, and V. Vitelli, Pattern formation by turbulent cascades, Nature (London) **627**, 515 (2024).
[57] C. B. Caporusso, G. Gonnella, and D. Levis, Phase coexistence and edge currents in the chiral Lennard-Jones fluid, Phys. Rev. Lett. **132**, 168201 (2024).
[58] H. Tanaka and T. Araki, Simulation method of colloidal suspensions with hydrodynamic interactions: Fluid particle dynamics, Phys. Rev. Lett. **85**, 1338 (2000).
[59] A. Furukawa, M. Tateno, and H. Tanaka, Physical foundation of the fluid particle dynamics method for colloid dynamics simulation, Soft Matter **14**, 3738 (2018).
[60] See Supplemental Material at http://link.aps.org/supplemental/10.1103/PhysRevResearch.6.023186 for the additional characterization of pattern formation and domain coarsening.
[61] K. Drescher, J. Dunkel, L. H. Cisneros, S. Ganguly, and R. E. Goldstein, Fluid dynamics and noise in bacterial cell–cell and cell–surface scattering, Proc. Natl. Acad. Sci. USA **108**, 10940 (2011).
[62] D. Pine, N. Easwar, J. V. Maher, and W. I. Goldburg, Turbulent suppression of spinodal decomposition, Phys. Rev. A **29**, 308 (1984).
[63] J. A. Aronovitz and D. R. Nelson, Turbulence in phase-separating binary mixtures, Phys. Rev. A **29**, 2012 (1984).
[64] P. Tong, W. I. Goldburg, J. Stavans, and A. Onuki, Temporal fluctuations in a turbulently stirred binary liquid mixture, Phys. Rev. Lett. **62**, 2668 (1989).
[65] L. Berthier, J.-L. Barrat, and J. Kurchan, Phase separation in a chaotic flow, Phys. Rev. Lett. **86**, 2014 (2001).
[66] S. Berti, G. Boffetta, M. Cencini, and A. Vulpiani, Turbulence and coarsening in active and passive binary mixtures, Phys. Rev. Lett. **95**, 224501 (2005).

[67] M. Seul and D. Andelman, Domain shapes and patterns: The phenomenology of modulated phases, Science **267**, 476 (1995).

[68] D. Andelman and R. E. Rosensweig, Modulated phases: Review and recent results, J. Phys. Chem. B **113**, 3785 (2009).

[69] H. Furukawa, Effect of inertia on droplet growth in a fluid, Phys. Rev. A **31**, 1103 (1985).

[70] S. Torquato and H. W. Haslach Jr, Random heterogeneous materials: Microstructure and macroscopic properties, Appl. Mech. Rev. **55**, B62 (2002).

[71] A. Alexakis and L. Biferale, Cascades and transitions in turbulent flows, Phys. Rep. **767-769**, 1 (2018).

[72] P. Perlekar, N. Pal, and R. Pandit, Two-dimensional turbulence in symmetric binary-fluid mixtures: Coarsening arrest by the inverse cascade, Sci. Rep. **7**, 44589 (2017).

[73] V. M. Kendon, J. C. Desplat, P. Bladon, and M. E. Cates, 3D spinodal decomposition in the inertial regime, Phys. Rev. Lett. **83**, 576 (1999).

[74] V. M. Kendon, M. E. Cates, I. Pagonabarraga, J.-C. Desplat, and P. Bladon, Inertial effects in three-dimensional spinodal decomposition of a symmetric binary fluid mixture: A lattice Boltzmann study, J. Fluid Mech. **440**, 147 (2001).

[75] P. Perlekar, R. Benzi, H. J. H. Clercx, D. R. Nelson, and F. Toschi, Spinodal decomposition in homogeneous and isotropic turbulence, Phys. Rev. Lett. **112**, 014502 (2014).